
Article:
Boehm, M., Lawrie, A. orcid.org/0000-0003-4192-9505, Wilhelm, J. et al. (6 more authors) (2016) Maintained right ventricular pressure overload induces ventricular-arterial decoupling in mice. Experimental Physiology. ISSN 0958-0670

https://doi.org/10.1113/EP085963

Maintained right ventricular pressure overload induces ventricular-arterial decoupling in mice

Brief title: Boehm et al. PAB-induces VA decoupling in mice

Mario Boehm MSc; Allan Lawrie PhD; Jochen Wilhelm PhD; Hossein A. Ghofrani MD; Friedrich Grimminger MD, PhD; Norbert Weissmann PhD; Werner Seeger MD; Ralph T. Schermuly PhD; Baktybek Kojonazarov MD, PhD

From the Universities of Giessen and Marburg Lung Center (UGMLC), Excellence Cluster Cardio-Pulmonary System (ECCPS), Member of the German Center for Lung Research (DZL), Giessen, Germany (M.B., J.W., H.A.G., F.G., N.W., R.T.S., B.K.), the Max Planck Institute for Heart and Lung Research, Bad Nauheim, Germany (W.S.) and the Pulmonary Vascular Research Group, Department of Infection, Immunity and Cardiovascular Disease, University of Sheffield, Sheffield, United Kingdom (A.L.).

REPRINT REQUEST AND CORRESPONDENCE:
Professor Ralph T. Schermuly and Dr. Baktybek Kojonazarov
Universities of Giessen and Marburg Lung Center (UGMLC)
Member of the German Center for Lung Research (DZL)
Aulweg 130, 35392 Giessen
Germany
Phone: +49 641 9942420
Fax: +49 641 9942419
e-mail: ralph.schermuly@innere.med.uni-giessen.de
e-mail: baktybek.kojonazarov@innere.med.uni-giessen.de

Total number of words: 3483

Total number of references: 50

Key words: Pulmonary hypertension, Right ventricle, Ventricular-arterial coupling,

Summary statement:

This is an Accepted Article that has been peer-reviewed and approved for publication in the Experimental Physiology, but has yet to undergo copy-editing and proof correction. Please cite this article as an Accepted Article; doi: 10.1113/EP085963.

Complementary utilization of echocardiographic imaging along with pressure-volume catheterization reveals ventricular-arterial decoupling of the pressure overloaded right ventricle in mice.

Abstract

New Findings:

What is the central question of this study?

The aim is to investigate whether complementary assessment of non-invasive ultrasound imaging along with closed chest-derived intra-cardiac pressure-volume catheterization is applicable to mice for an in-depth characterization of right ventricular (RV) function even upon maintained pressure overload.

What is the main finding and its importance?

Characterization of RV function by the complementary utilization of echocardiographic imaging along with pressure-volume catheterization reveals ventricular-arterial decoupling upon maintained pressure overload where RV systolic function correlates rather with ventricular-arterial coupling than contractility while diastolic function well correlates with RV diastolic pressure. This combinational approach allows us to better phenotype RV function/dysfunction in genetically modified and/or pharmacologically treated mice.

Assessment of right ventricular (RV) function in rodents is a challenge due to the complex RV anatomy and structure. Subsequently, the best characterization of RV function is achieved by accurate cardiovascular phenotyping, involving a combination of non-invasive imaging and intra-cardiac pressure-volume measurements. We sought to investigate the feasibility of two complementary phenotyping techniques for the evaluation of RV function in an experimental mouse model of sustained RV pressure overload. Mice underwent either Sham surgery (n=5) or pulmonary artery banding (PAB) (n=8) to induce isolated RV pressure overload. After three weeks indices of RV function were assessed by echocardiography (Vevo2100) and closed chest-derived invasive pressure-volume

measurements (PVR-1030). PAB resulted in RV hypertrophy and dilatation accompanied by systolic and diastolic dysfunction. Invasive RV hemodynamic measurements demonstrate an increased end-systolic as well as arterial elastance after PAB as compared to sham, resulting in ventricular-arterial decoupling. Regression analysis revealed that TAPSE is rather correlated with ventricular-arterial coupling (r^2=0.77, p=0.002) than RV contractility (r^2=-0.61, p=0.07). Furthermore, IVRT/RR and E/E' correlate well with RV end-diastolic pressure (r^2=0.87, p=0.0001 and r^2=0.82, p=0.0009; respectively). Commonly used indices of systolic RV function are associated with RV-arterial coupling rather than contractility, while diastolic indices are interrelated with end-diastolic pressure where there is maintained pressure overload.

Introduction

Right ventricular (RV) failure due to sustained pressure overload is the major cause of mortality in patients suffering from congenital heart diseases and pulmonary arterial hypertension (PAH) (Bogaard *et al.*, 2009*a*; Naeije & Manes, 2014). PAH itself is characterized by a progressive elevation of pulmonary vascular resistance leading to RV hypertrophy and ultimately RV failure in most patients (Schermuly *et al.*, 2011; Rabinovitch, 2012), while a subgroup of patients adapt with a compensated RV hypertrophy without immediate RV failure (Rich *et al.*, 2010). Consequently, the accurate assessment of RV indices by non-invasive imaging along with intra-cardiac measures are essential to diagnose rising filling pressures, diastolic dysfunction and reduced ejection volumes (Voelkel *et al.*, 2006; Pokreisz *et al.*, 2007; Borgdorff *et al.*, 2015*b*).

Pre-clinically, the precise characterization of RV function in rodents is hampered by the complex RV geometry. However, the availability of genetically modified mice allows performing more detailed pharmacological and molecular-mechanistic studies to better understand the physiology and pathology of the human disease. Furthermore, as miniature sensor technology progresses, first studies assessing simultaneous RV pressure and volume in small animals via open-chest approaches

were reported (Faber *et al.*, 2006; Bartelds *et al.*, 2011; Kapur *et al.*, 2013; Borgdorff *et al.*, 2013, 2015*b*; de Raaf *et al.*, 2015; Szulcek *et al.*, 2016). However, opening the chest and insertion of the catheter through the RV free wall cause loss of intrathoracic pressure, changes of myocardial integrity and trauma.

Evidence from experimental PAH suggests that pulmonary artery banding (PAB) challenged animals develop pressure overload-induced compensatory RV hypertrophy (Bogaard *et al.*, 2009*b*) or RV failure (Borgdorff *et al.*, 2015*b*), depending on the severity of pulmonary artery constriction and duration of maintained RV pressure overload. PAB is an animal model that induces isolated shear stress on the RV myocardium without affecting the pulmonary circulation which recently has drawn more attention.

To date, there have been no data reported that describe load-dependent and load-independent indices of systolic as well as diastolic RV function by the complementary usage of non-invasive imaging along with closed chest-derived invasive pressure-volume determinations, particularly in mice subjected to PAB. Thus, we hypothesized that the combination of trans-thoracic echocardiographic imaging along with closed chest-derived intra-cardiac pressure-volume measurements is feasible and allows for assessment of RV indices in mice - even upon three weeks of sustained RV pressure overload by PAB.

Methods

Ethical approval

All Experiments were performed according to institutional guidelines that comply with national and international regulations (EU directive 2010/63). The local authorities for animal research approved the study protocol (Regierungspräsidium Giessen).

Experimental protocol

Male C57BL/6 mice with a body weight of 20 ± 2 g (12 weeks of age) were obtained from Charles River Laboratories (Sulzfeld, Germany) and randomized into two groups: group 1, Sham-operated controls (n=5 mice) or group 2, chronic pulmonary artery banded (PAB) animals (n=8 mice). All mice were kept under identical housing conditions, underwent echocardiographic analysis and terminal hemodynamic evaluation three weeks upon surgery.

Pulmonary artery banding (PAB)

Pulmonary artery banding (PAB) was performed as described previously by our group (Novoyatleva *et al*., 2013; Kojonazarov *et al*., 2013; Janssen *et al*., 2015). Briefly, animals received a subcutaneous injection of 0.05 mg/kg buprenorphine hydrochloride for analgesia, were anesthetized by continuous isoflurane inhalation (2.0-2.5 % mixed in 100 % oxygen), intubated and mechanically ventilated. Subsequently, when animals lost their pedal withdrawl reflex and muscles relaxed – suggesting medium plane of anesthesia – the main pulmonary artery was constricted with a small titanium ligating clip (Hemoclip; Edward Weck, Research Triangle Park, NC) to a width of 0.3 mm in diameter after which the chest was closed and the animals allowed recovering. Sham control mice were subjected to equally performed surgery except applying the clip to the pulmonary artery. Post-operative analgesia was maintained by administration of 4 mg/kg carprofen mixed in drinking water.

Echocardiography

Transthoracic echocardiography was performed by an experienced sonographer in a blinded manner with a Vevo2100 system (Visualsonics, Toronto, Canada) to measure RV wall thickness (RVWT), RV internal diameter (RVID) and TAPSE as described previously (Savai *et al*., 2014). Pulmonary artery (PA) velocity time integral (VTI) was measured from the pulsed-wave Doppler flow velocity profile of the RV outflow tract in the parasternal short-axis view. By combining PA VTI, pulmonary artery area and heart rate, the echocardiographically derived cardiac output (CO) was determined in sham and PAB mice. Cardiac index (CI; ml min^{-1} body $weight^{-1}$) was calculated as cardiac output (CO; ml min^{-1}) normalized to body weight. The transtricuspidal early diastolic E-wave peak velocity was recorded from the apical four-chamber view. Tissue Doppler imaging (TDI) was used to measure early (E') diastolic peak velocity at the lateral corner of the tricuspid annulus. TDI-derived isovolumic relaxation time (IVRT), isovolumic contraction time (IVCT) and ejection time (ET) were measured and myocardial performance index (MPI) was calculated as a sum of IVRT and IVCT divided to ET.

Catheterization

All animals underwent terminal hemodynamic evaluation by pressure-volume analysis in blinded fashion. Mice were anaesthetized via sustained isoflurane inhalation (1.5-2 %) and core body temperature was maintained constant at 37° C

during the whole experiment. Prior to data recordings, the catheter was zeroed in pre-warmed saline using appropriate MPVSultra software (ADinstruments, Oxford, UK). Subsequently, the right external jugular vein was cannulated in all animals by the same single segment pressure-volume catheter (PVR1030, ADinstruments, Oxford, UK) connected to a MPVSultra pressure-volume unit to record relative volume units (RVUs), advanced into the RV and once in longitudinal position, steady-state signals were recorded (2k/s sampling rate). The end-systolic pressure-volume relation (ESPVR) was recorded during transient preload reduction through inferior vena cava (IVC) occlusion utilizing a cotton tipped applicator (871-PC DBL, Puritan, Maine, USA). Then, the same catheter was pulled out of the RV and used to cannulate the right carotid artery, introduced into the aorta and systemic blood pressure recorded. Terminally, all mice were euthanized by exsanguination and the RVs dissected from left ventricle (LV) and interventricular septum (S) for tissue weight measurements.

Data analysis

Hemodynamic data analysis was performed in Labchart software (ADinstruments, Oxford, UK). Therefore, in every mouse, echocardiographically determined stroke volume (in µl) was utilized to calibrate the catheter-derived arbitrary conductance signal into catheter-derived stroke volume in µl and in combination with heart rate into cardiac output (CO) as it was described before (Faber *et al.*, 2006; Borgdorff *et al.*, 2012; Andersen *et al.*, 2014). End-systolic elastance (Ees) was calculated as slope of ESPVR and arterial elastance (Ea) was computed from RV end-systolic pressure divided by stroke volume. Ventricular-arterial coupling efficiency is defined as Ees to Ea ratio.

Statistics

All data are presented as mean±SD. Statistical comparison of two groups for significance was performed by two-tailed unpaired student's t test. Correlation was analyzed using Spearman's correlation calculated in GraphPad Prism software (La Jolla, CA, USA).

Results

Sustained RV pressure overload results in RV hypertrophy and dysfunction

First, we did not detect post-operative mortality neither in sham or PAB-challenged mice. Three weeks after surgery we evaluated whether chronic RV pressure overload induced RV hypertrophy and dysfunction (Table 1). Notably, PAB-challenged mice tended to decrease in bodyweight as compared to sham operated controls (23.25±1.41 vs. 25.00±1.87 g, $p>0.05$). However, in comparison with sham controls, three weeks of sustained RV pressure overload resulted in a significant increase in RV hypertrophy determined as RV/(LV+S) ratio (0.37±0.07 vs. 0.20±0.02, $p=0.0003$) and RV dysfunction reflected by reduced cardiac index (0.38±0.11 vs. 0.58±0.03 $ml \cdot min^{-1} \cdot BW^{-1}$, $p=0.003$) without affecting systemic blood pressure (70.77±8.02 vs. 79.10±3.09 mmHg, $p>0.05$) nor heart rate (439.60±38.90 vs. 481.80±19.64 bpm, $p>0.05$) (Table 1).

Echocardiographic evaluation indicates RV hypertrophy, dilatation and both, systolic as well as diastolic dysfunction

Second, we utilized non-invasive trans-thoracic ultrasound imaging to characterize RV function. Robust RV hypertrophy was indicated by raised RV wall thickness (0.54±0.09 vs. 0.26±0.04 mm, $p<0.0001$) (Figure 1A) accompanied by impaired RV systolic function as demonstrated by diminished TAPSE (1.04±0.11 vs. 1.44±0.06 mm, $p<0.0001$) (Figure 1B) upon PAB as compared with sham operated controls. Furthermore, three weeks of maintained RV pressure overload in comparison with sham control caused RV dilatation as RV internal diameter increased significantly (2.36±0.32 vs. 1.59±0.10 mm, $p<0.001$) (Figure 1C). These changes were compounded by impairment of diastolic function shown via increased isovolumic relaxation time (IVRT/RR, 16.00±1.46 vs. 11.37±1.08 %, $p<0.0001$) (Figure 1D) and ratio of the early diastolic peak velocity measured by Pulsed wave Doppler (E peak) to early diastolic peak obtained during Tissue Doppler Imaging (E' peak) (E/E', 22.41±4.94 vs. 10.81±1.72, $p=0.0004$) (Figure 1E) plus impaired global cardiac function determined by myocardial performance index (0.88±0.10 vs. 0.60±0.05, $p<0.02$) (Figure 1F), a parameter indicating both systolic and diastolic RV function.

Pressure-volume analysis demonstrates RV systolic as well as diastolic dysfunction, hyper-contractility and ventricular-arterial decoupling

Subsequent to echocardiographic evaluation, intra-cardiac pressure-volume measurements were performed to invasively assess RV hemodynamics. Therefore and as invasive pressure-volume measurements are highly dependent on accurate

catheter placement along the RV longitudinal axis, we utilized ultrasound to guide the catheter into the correct position avoiding direct contact with the RV free wall nor IVS during the whole cardiac cycle.

Three weeks of isolated RV pressure overload robustly induced RV hypertrophy as RV/BW increased significantly (1.11±0.22 vs. 0.70±0.05 $mg \cdot g^{-1}$, p=0.01) (Figure 2A), accompanied by elevated RV systolic (RVSP: 57.38±11.85 vs. 24.60±4.02 mmHg, p=0.0001) (Figure 2B) and diastolic (RVDP: 3.56±1.91 vs. 0.55±0.18 mmHg, p=0.01) (Figure 2C) pressures as compared to sham controls. These changes were compounded by a reduced stroke volume (20.72±7.17 vs. 30.14±1.84 µl, p<0.05) (Figure 2D) despite RV hyper-contractility (Ees: 1.64±0.86 vs. 0.62±0.20 $mmHg \cdot \mu l^{-1}$, p<0.04) (Figure 2E) upon PAB. The afterload, partially reflected by arterial elastance (3.15±1.49 vs. 0.82±0.14 $mmHg \cdot \mu l^{-1}$, p=0.01) (Figure 2F), increased more than three times upon maintained PAB resulting in arterial-ventricular decoupling (Ees/Ea: 0.53±0.13 vs. 0.77±0.24, p<0.04) (Figure 2G). Representative steady-state pressure-volume loops as well as continuous data collection during transient preload reduction revealed obvious differences between Sham- and PAB-challenged mice (Figure 2H).

RV systolic function correlates with arterial-ventricular coupling rather than contractility while RV diastolic function interrelates with diastolic pressure

Non-invasively determined TAPSE as an indicator of systolic RV function showed borderline interrelation with pressure-volume loop-derived contractility index end-systolic elastance (Ees, r^2=-0.61, p=0.07) (Figure 3A). However, TAPSE most accurately positively correlated with ventricular-arterial coupling (Ees/Ea, r^2=0.77, p=0.002) (Figure 3B). Non-invasively assessed isovolumic relaxation time (IVRT/RR, r^2=0.87, p=0001) (Figure 3C) and E/E' (r^2=0.82, p=0.0009) (Figure 3D) are well correlated with RV diastolic pressure.

Discussion

Within this study, we characterized RV function by non-invasive ultrasound imaging along with invasive intra-cardiac hemodynamic measures in mice. We demonstrate the feasibility of complementary assigning echocardiographic evaluation together with closed chest-derived pressure-volume measurements for the characterization of RV function in mice with sustained RV pressure overload-induced hypertrophy. We

also report, that RV systolic function in mice correlates with ventricular-arterial coupling rather than RV contractility, while RV diastolic function interrelates with end-diastolic pressure.

In many experimental studies in the literature, data interpretation is hampered by the lack of RV pressure-volume analysis (Borgdorff *et al.*, 2015*a*) which remains the gold standard to assess the RV response to pressure overload (Vogel, 2008; Chesler *et al.*, 2009; Spruijt *et al.*, 2014; Voelkel *et al.*, 2015). Indeed, the use of pressure-volume analysis as means of load-independent contractility measurements has long time been restricted to the LV since RV anatomy aggravates accurate conductance signal acquisition. Indeed, under conditions with normal RV pressure and function it is challenging to generate reliable data but upon even modestly elevated load, the RV shape resembles the more spherical LV unburden pressure-volume measurements. In our study, we utilized conventional echocardiographic-derived RV stroke volume and heart rate to convert it into cardiac output and calibrate the catheter-derived conductance signal. We determine end-systolic elastance during preload reduction, as cardiac output *per se* does not reflect contractility due to its load-dependency. Accordingly, several clinical and pre-clinical studies demonstrate that pressure-volume loop-derived analysis of RV contractility by end-systolic elastance - even calculated by single-beat estimation (Brimioulle *et al.*, 2003) - is a very sensitive tool providing greater insights into RV function or dysfunction, that may not be recognized by conventional catheterization (Faber *et al.*, 2006; Vogel, 2008; Spruijt *et al.*, 2014). Therefore, we went further and evaluated RV function by the complementary assignment of non-invasive ultrasound imaging along with closed chest-derived pressure-volume catheterization in mice.

There is now considerable evidence that emphasizes a significant role for RV contractility and decoupling of the ventricular-arterial system in PAH (Kuehne *et al.*, 2004; Pagnamenta *et al.*, 2010; Sanz *et al.*, 2012; Spruijt *et al.*, 2015). It was shown that ventricular-arterial coupling predicts outcome in PH patients (Vanderpool *et al.*, 2015) and further clinical data indicate that progression of PAH-associated RV dysfunction leads to RV failure with increased RV contractility but importantly, impaired RV ventricular-coupling in most patients (Kuehne *et al.*, 2004; Galie *et al.*, 2007), while a subgroup of patients adapt with preserved contractility and compensated RV hypertrophy (Rich *et al.*, 2010; Tedford *et al.*, 2013). Accordingly, a

recently published experimental study by Borgdorff and co-workers demonstrates that rats develop either clinical signs of heart failure upon tight pulmonary artery banding or adapt without signs of heart failure (Borgdorff *et al.*, 2015*b*). Importantly, while indices of systolic function deteriorate upon chronic pressure-overload as compared with sham-operated animals, pressure-volume loop-derived contractility measures indicate a hyper-contractile RV – even in animals with clinical signs of heart failure – accompanied by ventricular-arterial decoupling. Basically, optimal coupling efficiency is achieved if contractility is matched to vascular load (Naeije & Manes, 2014). Pulmonary artery constriction selectively elevates RV afterload leading to a hyper-contractile response of the RV which was also shown at different time points after pressure overload induction in other species (Leeuwenburgh *et al.*, 2002; Gaynor *et al.*, 2005; Apitz *et al.*, 2012). These and our data suggest that the observed contractility elevation together with RV dilatation and hypertrophy is insufficient to compensate for a dramatically increased afterload leading to ventricular-arterial decoupling and diminished RV ejection volumes.

In our study, pulmonary artery constriction was moderate and did not lead to very severe RV failure three weeks upon disease commencement. However, in accordance with the previously published experimental studies (Egemnazarov *et al.*, 2015; Kapur *et al.*, 2013; Janssen *et al.*, 2015), we herein demonstrate that chronic pressure overload resulted in RV hypertrophy, dilatation, impaired systolic as well as diastolic function and increased RV contractility accompanied by ventricular-arterial decoupling.

Interestingly, couple of studies in experimental PAH models demonstrate preserved ventricular-arterial coupling with contractility elevation that match the increased afterload thereby maintaining RV ejection volumes (Wauthy *et al.*, 2004; Fesler *et al.*, 2006; Rex *et al.*, 2008) while others indicate decoupling and reduced RV output (Kerbaul *et al.*, 2004, 2006, 2007; Missant *et al.*, 2007; Pagnamenta *et al.*, 2010; Rondelet *et al.*, 2012). Here, we can speculate that severity of afterload elevation, duration of progressive RV pressure overload and species may account for these differences.

Previous work has also been shown that metabolic adaptation to chronic hypoxia unaffected ventricular-arterial coupling in mice (10 days, 10% O_2) (Tabima *et al.*, 2010; Schreier *et al.*, 2013). Furthermore, it was demonstrated that in the mouse

model of Sugen5416 injection followed by 28 days of chronic hypoxia that hypoxic adaptation had no effect on ventricular-arterial coupling (Wang *et al.*, 2013). These effects were measured by admittance technology and open-chest approaches. As chronic hypoxia primarily results in vasoconstriction of pulmonary vessels with compensatory RV adaptation that can be reversed by re-exposure to normoxia, we thought to investigate whether progressive high RV wall stress *per se* affects ventricular-arterial coupling in mice.

Guihaire and co-authors demonstrated in a porcine model of chronic pressure overload that non-invasively assessed indices of RV function rather interrelate with ventricular-arterial coupling than contractility (Guihaire *et al.*, 2013). In our study, regression analyses support this observation by demonstration of better correlation between non-invasively assessed TAPSE with ventricular-arterial coupling than contractility. Furthermore, we show that non-invasive indices of diastolic function well correlate with RV end-diastolic pressure. This is conform with experimental and clinical data out of the literature indicating that RV diastolic stiffness contributes to functional impairment of the RV in pulmonary arterial hypertension (Egemnazarov *et al.*, 2015; Rain *et al.*, 2013).

There are several limitations to this study. First, the usage of a retrograde technique for catheter insertion into the RV longitudinal axis may account for small changes in RV volumes as tricuspid regurgitation may occur. Second, cardiac output determination by conventional echocardiography may not reflect absolute RV volumes due to weaknesses of this technique leading to vague conductance calibration. Third, the catheter-derived conductance signal may comprise blood and partially myocardial muscle resistivity.

All together, our ability to deeply characterize RV function and ventricular-arterial coupling in mice – even after chronic pressure overload – will allow us to better phenotype genetically modified animals and to explore the effects of pharmacological compounds in the setting of isolated RV pressure overload-induced dysfunction and failure. Future studies employing more follow-up time points upon pulmonary artery constriction in mice are warranted that may further define the course of RV remodeling, ventricular-arterial decoupling and the development of RV failure in response to PAH-associated RV pressure overload.

Competing interest: none declared

Author contributions: Design of the work: M.B., A.L., W.S., R.T.S., B.K. Acquisition of data: M.B., B.K. Analysis of data: M.B., J.W., B.K. Interpretation of data: M.B., A.L., J.W., H.A.G., F.G., N.W., W.S., R.T.S., B.K. Drafting the manuscript: M.B., B.K. Critical revision: A.L., J.W., H.A.G., F.G., N.W., W.S., R.T.S All authors approved the final version of the manuscript and agree to be accountable for all aspects of the work in ensuring that questions related to the accuracy or integrity of any part of the work are appropriately investigated and resolved. All persons designated as authors qualify for authorship, and all those who qualify for authorship are listed.

Funding: This study was supported by Universities of Giessen and Marburg Lung Center (UGMLC), Excellence Cluster Cardio-Pulmonary System and Collaborative Research Center 1213 (CRC1213).

References

Andersen S, Schultz JG, Andersen A, Ringgaard S, Nielsen JM, Holmboe S, Vildbrad

MD, de Man FS, Bogaard HJ, Vonk-Noordegraaf A & Nielsen-Kudsk JE (2014). Effects of bisoprolol and losartan treatment in the hypertrophic and failing right heart. *J Card Fail* **20,** 864–873.

Apitz C, Honjo O, Humpl T, Li J, Assad RS, Cho MY, Hong J, Friedberg MK & Redington AN (2012). Biventricular structural and functional responses to aortic constriction in a rabbit model of chronic right ventricular pressure overload. *J Thorac Cardiovasc Surg* **144,** 1494–1501.

Bartelds B, Borgdorff MA, Smit-Van Oosten A, Takens J, Boersma B, Nederhoff MG, Elzenga NJ, Van Gilst WH, De Windt LJ & Berger RMF (2011). Differential responses
of the right ventricle to abnormal loading conditions in mice: Pressure vs. volume load. *Eur J Heart Fail* **13,** 1275–1282.

Bogaard HJ, Abe K, Vonk Noordegraaf A & Voelkel NF (2009*a*). The right ventricle under pressure: cellular and molecular mechanisms of right-heart failure in pulmonary hypertension. *Chest* **135,** 794–804.

Bogaard HJ, Natarajan R, Henderson SC, Long CS, Kraskauskas D, Smithson L, Ockaili R, McCord JM & Voelkel NF (2009*b*). Chronic pulmonary artery pressure elevation is insufficient to explain right heart failure. *Circulation* **120,** 1951–1960.

Borgdorff M a. J, Dickinson MG, Berger RMF & Bartelds B (2015*a*). Right ventricular failure due to chronic pressure load: What have we learned in animal models since the NIH working group statement? *Heart Fail Rev*; DOI: 10.1007/s10741-015-9479-6.

Borgdorff MA, Bartelds B, Dickinson MG, Steendijk P & Berger RMF (2013). A cornerstone of heart failure treatment is not effective in experimental right ventricular failure. *Int J Cardiol* **169,** 183–189.

Borgdorff MAJ, Bartelds B, Dickinson MG, Boersma B, Weij M, Zandvoort A, Sillj?? HHW, Steendijk P, De Vroomen M & Berger RMF (2012). Sildenafil enhances systolic adaptation, but does not prevent diastolic dysfunction, in the pressure-loaded
right ventricle. *Eur J Heart Fail* **14,** 1067–1074.

Borgdorff MAJ, Koop AMC, Bloks VW, Dickinson MG, Steendijk P, Sillje HHW, Van Wiechen MPH, Berger RMF & Bartelds B (2015*b*). Clinical symptoms of right ventricular failure in experimental chronic pressure load are associated with progressive diastolic dysfunction. *J Mol Cell Cardiol* **79,** 244–253.

Brimioulle S, Wauthy P, Ewalenko P, Rondelet B, Vermeulen F, Kerbaul F & Naeije R (2003). Single-beat estimation of right ventricular end-systolic pressure-volume relationship. *Am J Physiol Heart Circ Physiol* **284,** H1625–H1630.

Chesler NC, Roldan A, Vanderpool RR & Naeije R (2009). How to measure pulmonary vascular and right ventricular function. *Conf Proc . Annu Int Conf IEEE Eng Med Biol Soc IEEE Eng Med Biol Soc Annu Conf* **2009,** 177–180.

Egemnazarov B, Schmidt A, Crnkovic S, Sydykov A, Nagy BM, Kovacs G, Weissmann N & Olschewski H (n.d.). Pressure Overload Creates Right Ventricular Diastolic Dysfunction in a Mouse Model : Assessment by Echocardiography. 1–16.

Faber MJ, Dalinghaus M, Lankhuizen IM, Steendijk P, Hop WC, Schoemaker RG, Duncker DJ, Lamers JMJ & Helbing W a (2006). Right and left ventricular function after chronic pulmonary artery banding in rats assessed with biventricular pressure volume loops. *Am J Physiol Heart Circ Physiol* **291,** H1580–H1586.

Fesler P, Pagnamenta A, Rondelet B, Kerbaul F & Naeije R (2006). Effects of

sildenafil on hypoxic pulmonary vascular function in dogs. *J Appl Physiol* **101,** 1085 1090.

Galie N, Manes A, Palazzini M, Negro L, Romanazzi S & Branzi A (2007). Pharmacological impact on right ventricular remodelling in pulmonary arterial hypertension. *Eur Hear J Suppl* **9,** H68–H74.

Gaynor SL, Maniar HS, Bloch JB, Steendijk P & Moon MR (2005). Right atrial and ventricular adaptation to chronic right ventricular pressure overload. *Circulation* **112,** I212–I218.

Guihaire J, Haddad F, Boulate D, Decante B, Denault AY, Wu J, Hervé P, Humbert M, Dartevelle P, Verhoye J-P, Mercier O & Fadel E (2013). Non-invasive indices of right ventricular function are markers of ventricular-arterial coupling rather than ventricular contractility: insights from a porcine model of chronic pressure overload. *Eur Heart J Cardiovasc Imaging* **14,** 1140–1149.

Janssen W, Schymura Y, Novoyatleva T, Kojonazarov B, Boehm M, Wietelmann A, Luitel H, Murmann K, Krompiec DR, Tretyn A, Pullamsetti SS, Weissmann N, Seeger W, Ghofrani HA & Schermuly RT (2015). 5-HT2B Receptor Antagonists Inhibit Fibrosis and Protect from RV Heart Failure. *Biomed Res Int* **2015,** 438403.

Kapur NK, Paruchuri V, Aronovitz MJ, Qiao X, Mackey EE, Daly GH, Ughreja K, Levine J, Blanton R, Hill NS & Karas RH (2013). Biventricular Remodeling in Murine Models of Right Ventricular Pressure Overload. *PLoS One*; DOI: 10.1371/journal.pone.0070802.

Kerbaul F, Brimioulle S, Rondelet B, Dewachter C, Hubloue I & Naeije R (2007). How prostacyclin improves cardiac output in right heart failure in conjunction with pulmonary hypertension. *Am J Respir Crit Care Med* **175,** 846–850.

Kerbaul F, Rondelet B, Demester J-P, Fesler P, Huez S, Naeije R & Brimioulle S (2006). Effects of levosimendan versus dobutamine on pressure load-induced right

ventricular failure. *Crit Care Med* **34,** 2814–2819.

Kerbaul F, Rondelet B, Motte S, Fesler P, Hubloue I, Ewalenko P, Naeije R & Brimioulle S (2004). Effects of norepinephrine and dobutamine on pressure load-induced right ventricular failure. *Crit Care Med* **32,** 1035–1040.

Kojonazarov B, Luitel H, Sydykov A, Dahal BK, Paul-Clark MJ, Bonvini S, Reed A, Schermuly RT & Mitchell JA (2013). The peroxisome proliferator-activated receptor β/δ agonist GW0742 has direct protective effects on right heart hypertrophy. *Pulm Circ* **3,** 926–935.

Kuehne T, Yilmaz S, Steendijk P, Moore P, Groenink M, Saaed M, Weber O, Higgins CB, Ewert P, Fleck E, Nagel E, Schulze-Neick I & Lange P (2004). Magnetic resonance imaging analysis of right ventricular pressure-volume loops: in vivo validation and clinical application in patients with pulmonary hypertension. *Circulation* **110,** 2010–2016.

Leeuwenburgh BPJ, Steendijk P, Helbing WA & Baan J (2002). Indexes of diastolic RV function: load dependence and changes after chronic RV pressure overload in lambs. *Am J Physiol Heart Circ Physiol* **282,** H1350–H1358.

Missant C, Rex S, Segers P & Wouters PF (2007). Levosimendan improves right ventriculovascular coupling in a porcine model of right ventricular dysfunction. *Crit Care Med* **35,** 707–715.

Naeije R & Manes A (2014). The right ventricle in pulmonary arterial hypertension. *Eur Respir Rev* **23,** 476–487.

Novoyatleva T, Schymura Y, Janssen W, Strobl F, Swiercz JM, Patra C, Posern G, Wietelmann A, Zheng TS, Schermuly RT & Engel FB (2013). Deletion of Fn14 receptor protects from right heart fibrosis and dysfunction. *Basic Res Cardiol* **108,** 325.

Pagnamenta A, Dewachter C, McEntee K, Fesler P, Brimioulle S & Naeije R (2010). Early right ventriculo-arterial uncoupling in borderline pulmonary hypertension on experimental heart failure. *J Appl Physiol* **109,** 1080–1085.

Pokreisz P, Marsboom G & Janssens S (2007). Pressure overload-induced right ventricular dysfunction and remodelling in experimental pulmonary hypertension: the right heart revisited. *Eur Hear J Suppl* **9,** H75–H84.

de Raaf MA, Kroeze Y, Middelman A, de Man FS, de Jong H, Vonk-Noordegraaf A, de Korte C, Voelkel NF, Homberg J & Bogaard HJ (2015). Serotonin transporter is not required for the development of severe pulmonary hypertension in the Sugen hypoxia rat model. *Am J Physiol Lung Cell Mol Physiol* **309,** L1164–L1173.

Rabinovitch M (2012). Molecular pathogenesis of pulmonary arterial hypertension. *J Clin Invest* **122,** 4306–4313.

Rain S et al. (2013). Right ventricular diastolic impairment in patients with pulmonary arterial hypertension. *Circulation* **128,** 2016–2025, 1–10.

Rex S, Missant C, Segers P, Rossaint R & Wouters PF (2008). Epoprostenol treatment of acute pulmonary hypertension is associated with a paradoxical decrease in right ventricular contractility. *Intensive Care Med* **34,** 179–189.

Rich S, Pogoriler J, Husain AN, Toth PT, Gomberg-Maitland M & Archer SL (2010). Long-term effects of epoprostenol on the pulmonary vasculature in idiopathic pulmonary arterial hypertension. *Chest* **138,** 1234–1239.

Rondelet B, Dewachter C, Kerbaul F, Kang X, Fesler P, Brimioulle S, Naeije R & Dewachter L (2012). Prolonged overcirculation-induced pulmonary arterial hypertension as a cause of right ventricular failure. *Eur Heart J* **33,** 1017–1026.

Sanz J, García-Alvarez A, Fernández-Friera L, Nair A, Mirelis JG, Sawit ST, Pinney S & Fuster V (2012). Right ventriculo-arterial coupling in pulmonary hypertension: a

magnetic resonance study. *Heart* **98,** 238–243.

Savai R, Al-Tamari HM, Sedding D, Kojonazarov B, Muecke C, Teske R, Capecchi MR, Weissmann N, Grimminger F, Seeger W, Schermuly RT & Pullamsetti SS (2014). Pro-proliferative and inflammatory signaling converge on FoxO1 transcription factor in pulmonary hypertension. *Nat Med* **20,** 1289–1300.

Schermuly RT, Ghofrani H a, Wilkins MR & Grimminger F (2011). Mechanisms of disease: pulmonary arterial hypertension. *Nat Rev Cardiol* **8,** 443–455.
Schreier D, Hacker T, Song G & Chesler N (2013). The role of collagen synthesis in ventricular and vascular adaptation to hypoxic pulmonary hypertension. *J Biomech Eng* **135,** 021018.

Spruijt OA, Bogaard H-J & Vonk-Noordegraaf A (2014). Assessment of right ventricular responses to therapy in pulmonary hypertension. *Drug Discov Today*; DOI: 10.1016/j.drudis.2014.03.008.

Spruijt OA, de Man FS, Groepenhoff H, Oosterveer F, Westerhof N, Vonk-Noordegraaf A & Bogaard H-J (2015). The effects of exercise on right ventricular contractility and right ventricular-arterial coupling in pulmonary hypertension. *Am J Respir Crit Care Med* **191,** 1050–1057.

Szulcek R, Happé CM, Rol N, Fontijn RD, Dickhoff C, Hartemink KJ, Grünberg K, Tu L, Timens W, Nossent GD, Paul MA, Leyen TA, Horrevoets AJ, de Man FS, Guignabert C, Yu PB, Vonk-Noordegraaf A, van Nieuw Amerongen GP & Bogaard HJ (2016). Delayed Microvascular Shear-adaptation in Pulmonary Arterial Hypertension: Role of PECAM-1 Cleavage. *Am J Respir Crit Care Med*; DOI: 10.1164/rccm.201506-1231OC.

Tabima DM, Hacker TA & Chesler NC (2010). Measuring right ventricular function in the normal and hypertensive mouse hearts using admittance-derived pressure-volume loops. *Am J Physiol Heart Circ Physiol* **299,** H2069–H2075.

Tedford RJ, Mudd JO, Girgis RE, Mathai SC, Zaiman AL, Housten-Harris T, Boyce D, Kelemen BW, Bacher AC, Shah AA, Hummers LK, Wigley FM, Russell SD, Saggar R, Saggar R, Maughan WL, Hassoun PM & Kass DA (2013). Right ventricular dysfunction in systemic sclerosis-associated pulmonary arterial hypertension. *Circ Heart Fail* **6,** 953–963.

Vanderpool RR, Pinsky MR, Naeije R, Deible C, Kosaraju V, Bunner C, Mathier MA, Lacomis J, Champion HC & Simon MA (2015). RV-pulmonary arterial coupling predicts outcome in patients referred for pulmonary hypertension. *Heart* **101,** 37–43.

Voelkel NF, Bogaard HJ & Gomez-Arroyo J (2015). The need to recognize the pulmonary circulation and the right ventricle as an integrated functional unit: facts and hypotheses (2013 Grover Conference series). *Pulm Circ* **5,** 81–89.

Voelkel NF, Quaife R a, Leinwand L a, Barst RJ, McGoon MD, Meldrum DR, Dupuis J, Long CS, Rubin LJ, Smart FW, Suzuki YJ, Gladwin M, Denholm EM & Gail DB (2006). Right ventricular function and failure: report of a National Heart, Lung, and Blood Institute working group on cellular and molecular mechanisms of right heart failure. *Circulation* **114,** 1883–1891.

Vogel M (2008). The optimal method with which to assess right ventricular function. *Cardiol Young* **9,** 547–548.

Wang Z, Schreier DA, Hacker TA & Chesler NC (2013). Progressive right ventricular functional and structural changes in a mouse model of pulmonary arterial hypertension. *Physiol Rep* **1,** e00184.

Wauthy P, Pagnamenta A, Vassalli F, Naeije R & Brimioulle S (2004). Right ventricular adaptation to pulmonary hypertension: an interspecies comparison. *Am J Physiol Heart Circ Physiol* **286,** H1441–H1447.

Figure Legends

Figure 1: Echocardiographic functional measurements

RV hypertrophy, measured as RV wall thickness (RVWT, mm) (**A**), tricuspid annular plane systolic excursion (TAPSE, mm) (**B**), RV dilatation, measured by RV internal diameter (RVID, mm) (**C**), isovolumic relaxation time to electrocardiogram-derived RR interval (IVRT/RR, %) (**D**), ratio of the transtricuspidal E peak velocity to tissue Doppler derived E' peak velocity (**E**), myocardial performance index (MPI, Tei index) (**F**) and representative echocardiographic measurements derived from sham- and PAB-challenged mice (**G**). Data are shown as mean±SD. for n=5 mice subjected to sham and n=8 mice to PAB surgery. Two-tailed unpaired student's t-test was used for two group comparison.

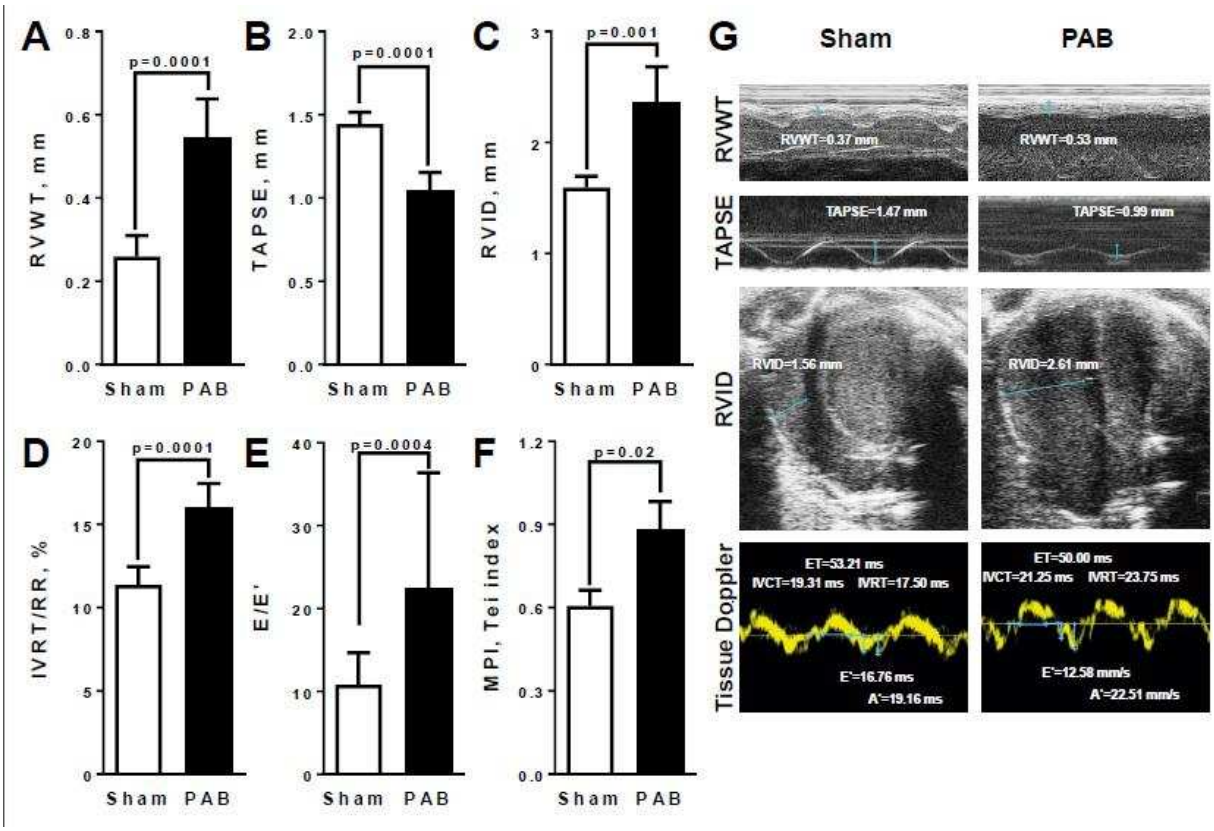

Figure 2: Hemodynamic characterization of RV function

RV hypertrophy, measured as ratio of RV to body weight (BW) (RV/BW) (**A**), RV systolic pressure (RVSP, mmHg) (**B**), RV diastolic pressure (RVDP, mmHg) (**C**), stroke volume (SV, µl) (**D**), RV contractility, measured as end-systolic elastance (Ees, mmHg·µl^{-1}) (**E**), arterial elastance (Ea, mmHg·µl^{-1}) (**F**) and representative continuous pressure-volume recordings during transient preload reduction (**G**). Data are shown as mean±SD. for n=5 mice subjected to sham and n=8 mice to PAB surgery. Two-tailed unpaired student's t-test was used for two group comparison.

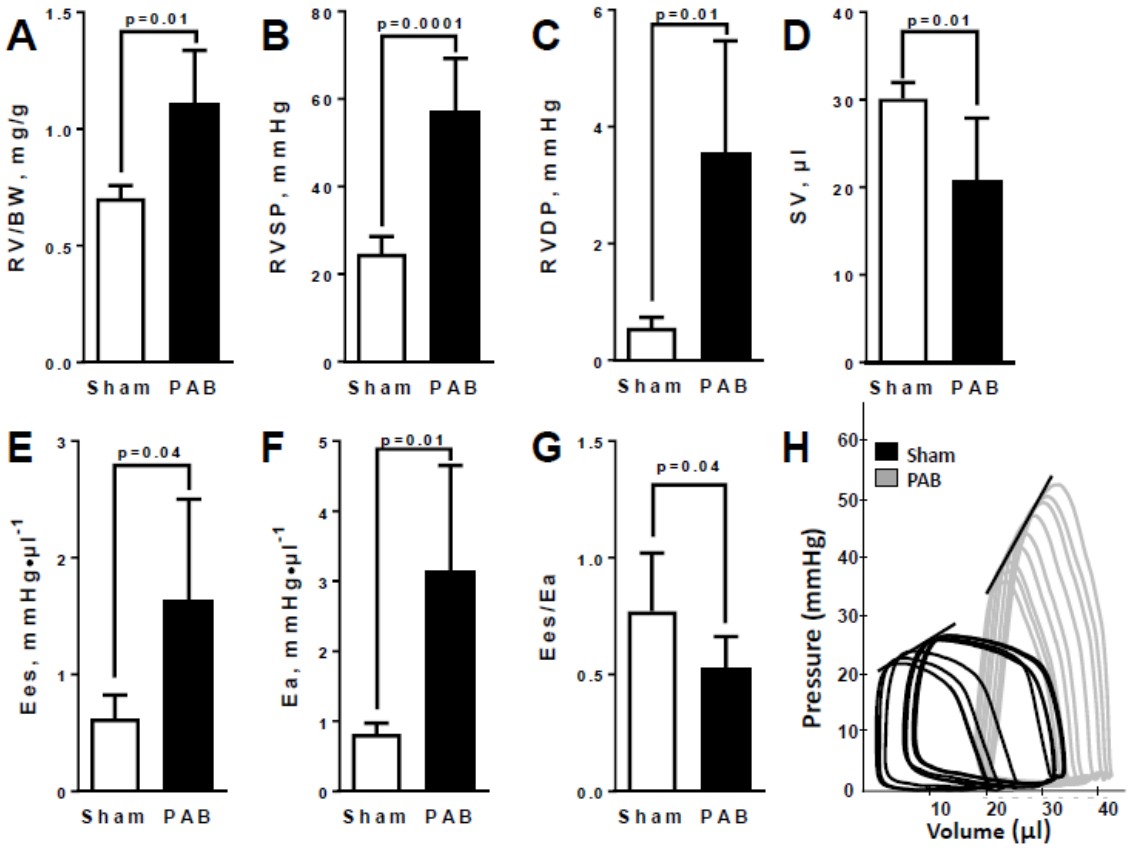

Figure 3: Linear regression analyses of non-invasively assessed RV systolic and diastolic indices versus invasively determined parameters in sham and PAB operated animals

Correlation between echocardiographically measured tricuspid annular plane systolic excursion (TAPSE, mm) and end-systolic elastance (Ees, mmHg·µl^{-1}) (**A**), interrelation between tricuspid annular plane systolic excursion (TAPSE, mm) and end-systolic elastance to arterial elastance ratio (Ees/Ea) (**B**), correlation between isovolumic relaxation time to electrocardiogram-derived RR interval (IVRT/RR, %) and RV diastolic pressure (RVDP, mmHg) (**C**), correlation between E/E' and RV diastolic pressure (RVDP, mmHg) (**D**). Spearman's correlation analysis, r²: goodness of fit. Two-tailed unpaired student's t-test was used for two group comparison.

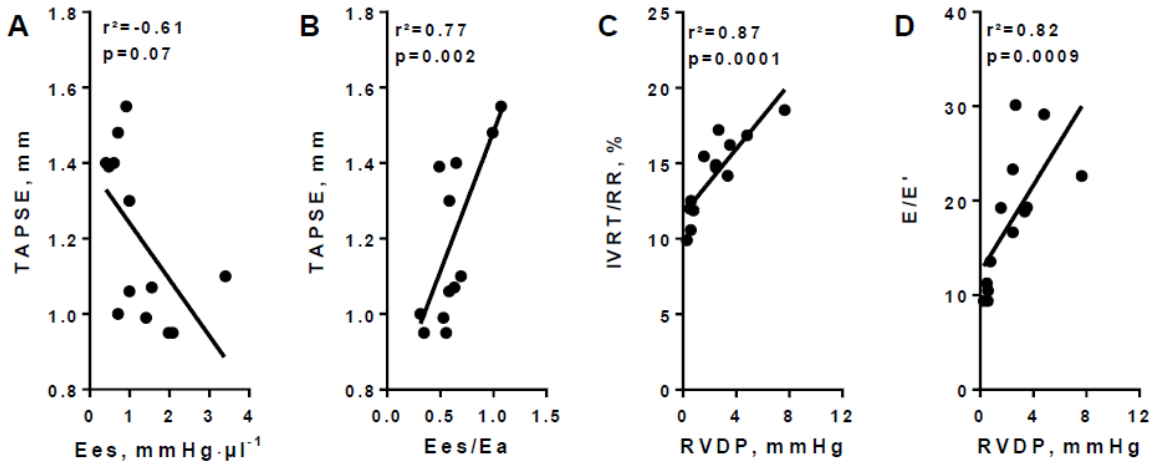

Table 1: Basic animal characteristics

	Sham	PAB	p-value
n, number	5	8	-
Body weight (day 0), g	21.50±0.79	21.25±0.88	ns.
Body weight (day 21), g	25.00±1.87	23.25±1.41	ns.
RV/(LV+S)	0.20±0.02	0.37±0.07	0.0003
Systemic blood pressure, mmHg	79.10±3.09	70.77±8.02	ns.
Heart rate, bpm	481.80±19.64	439.60±38.90	ns.
Cardiac index, $ml \cdot min^{-1} \cdot BW^{-1}$	0.58±0.03	0.38±0.11	0.003

g- gram, **ns.** – not significant, **RV** – right ventricle, **LV** – left ventricle, **S** – septum, **mmHg** – millimeter of mercury, **bpm** – beats per minute, **BW** – body weight. All parameters are expressed as mean±SD. The p-value was calculated by using two-tailed unpaired student's t-test.